INTERNATIONAL JOURNAL FOR NUMERICAL METHODS IN FLUIDS, VOL. 25, 803–823 (1997)

AN ADAPTIVE FINITE ELEMENT METHOD FOR FORCED CONVECTION

D. PELLETIER,* F. ILINCA AND É. TURGEON

CERCA (Centre for Research in Computation and its Applications) and École Polytechnique de Montréal, PO Box 6079, Succursale Centre-ville, Montréal, Québec H3C 3A7, Canada

SUMMARY

This paper presents an adaptive finite element method to solve forced convective heat transfer. Solutions are obtained in primitive variables using a high-order finite element approximation on unstructured grids. Two general-purpose error estimators are developed to analyse finite element solutions and to determine the characteristics of an improved mesh which is adaptively regenerated by the advancing front method. The adaptive methodology is validated on a problem with a known analytical solution. The methodology is then applied to heat transfer predictions for two cases of practical interest. Predictions of the Nusselt number compare well with measurements and constitute an improvement over previous results. © 1997 John Wiley & Sons, Ltd.

Int. J. Numer. Meth. Fluids, **25**: 803–823 (1997).

No. of Figures: 15. No. of Tables: 11. No. of References: 22.

KEY WORDS: incompressible; Navier–Stokes; heat transfer; adaptive FEM; forced convection

1. INTRODUCTION

Heat transfer by forced convection is of practical significance for many systems of engineering interest. Examples include heat exchangers, cooling processes in nuclear reactors, combustors and furnaces and cooling of electronic equipment. All these applications present the same challenge for computational methods: the location and extent of shear and thermal layers and stagnation points are very difficult to determine *a priori*. The net result is that achieving accurate solutions is very demanding on the part of the analyst. Furthermore, accurate prediction of the Nusselt number is a difficult task because it requires the computation of the temperature gradient at the wall. It is a well-known fact that if the temperature is interpolated with an accuracy of $O(h^n)$, the accuracy of its gradient, and hence of the Nusselt number, will be one order lower, $O(h^{n-1})$. It follows that while a mesh may be fine enough to yield acceptable velocity and temperature profiles, it may produce an insufficiently accurate heat flux estimate for practical purposes.

Most of the recent work on adaptive finite element methods has focused on improving the

* Correspondence to: D. Pelletier, CERCA and École Polytechnique de Montréal, PO Box 6079, Succursale Centre-ville, Montréal, Québec H3C 3A7, Canada.

Contract grant sponsor: Natural Science and Engineering Research Council of Canada.
Contract grant sponsor: Le Fonds FCAR de la Province de Québec.

CCC 0271–2091/97/070803–21 $17.50

Received 27 February 1995
Revised 22 November 1996

accuracy of the primary unknowns, i.e. velocity, temperature and pressure. Little has been done to assess the accuracy of derived fields (heat flux, skin friction). This paper focuses on the development of adaptive finite element methods that will result in improved heat flux computations. Such methods provide a powerful approach for accurately solving such complex problems, because grid points are automatically clustered in regions of rapid solution variation to improve the accuracy of heat flux predictions. In the present approach this is done in such a way as to result in a solution that is uniformly accurate throughout the flow domain. That is, momentum and heat fluxes are uniformly accurate. This tight control on the solution process makes it possible to obtain *numerically exact solutions* (grid-independent) to the Navier–Stokes and energy equations. The adaptive process also turns out to be cost-effective in the sense that the best numerical solution is obtained at nearly minimal computational cost.

While initial breakthroughs occurred nearly 10 years ago in compressible aerodynamics,[1] little work has been done on incompressible flows and even less on heat transfer problems. Proof-of-concept computations were reported in References 2 and 3. In References 4–9 the methodology proposed by the authors was quantitatively validated by solving flows with known analytical solutions and by computing cases for which experimental measurements were available. Cases treated covered isothermal laminar flows, heat transfer by free convection, conjugate heat transfer with variable fluid properties and turbulent free shear flows. Validation was done by comparing predicted and measured velocity and temperature fields. This paper presents a rigorous extension of the methodology to forced convective heat transfer problems, with special emphasis on the effect of adaption on the accuracy of the Nusselt number prediction.

The paper is organized as follows. First the governing equations and the finite element solver are reviewed. The methodology section describes the two error estimators and the adaptive remeshing strategy. The proposed methodology is then validated by solving problems with known analytical solutions to clearly quantify the accuracy improvements due to adaptivity. The method is then applied to the prediction of heat transfer in a grooved duct and in a suddenly expanded channel with and without cold fluid injection. Results are compared with experiments. The paper closes with conclusions.

2. MODELLING OF THE PROBLEM

2.1. Equations of motion

The flow is modelled by the Navier–Stokes, continuity and energy equations written as

$$\begin{aligned} \rho \mathbf{u} \cdot \nabla \mathbf{u} &= -\nabla p + \nabla \cdot \tau, \\ \nabla \cdot \mathbf{u} &= 0, \\ \rho c_{\mathrm{p}} \mathbf{u} \cdot \nabla T &= \nabla \cdot \mathbf{q}, \end{aligned} \tag{1}$$

where the stress tensor τ is defined by

$$\tau = \mu[\nabla \mathbf{u} + (\nabla \mathbf{u})^{\mathrm{T}}] \tag{2}$$

and $q = k \nabla T$. Appropriate boundary conditions complete the statement of the problem:

$$\begin{aligned} u &= u_0 \quad \text{on } \Gamma_u, \\ \tau \cdot \hat{n} - p\hat{n} &= \hat{t} \quad \text{on } \Gamma_{\hat{t}}, \end{aligned} \tag{3}$$

$$\begin{aligned} T &= T_0 \quad \text{on } \Gamma_T, \\ k \nabla T \cdot \hat{n} &= q_{\mathrm{B}} \quad \text{on } \Gamma_q, \end{aligned} \tag{4}$$

where Γ_u and Γ_T are the portions of the boundary where Dirichlet conditions are applied. Neumann conditions are applied on the remaining portions $\Gamma_{\hat{t}}$ and Γ_q.

2.2. Finite element solver

The variational equations solved by the finite element method are obtained by multiplying the above equations by appropriate test functions and integrating over the domain of interest. Application of the divergence theorem to the momentum and temperature diffusion term leads to the weak form

$$\begin{aligned}(\rho\mathbf{u}\nabla\cdot\mathbf{u},\mathbf{v})+a(\mathbf{u},\mathbf{v})-(p,\nabla\cdot\mathbf{v})&=\langle t^*,\mathbf{v}\rangle,\\ (s,\nabla\cdot\mathbf{u})&=0,\\ (\rho c_{\mathrm{p}}\mathbf{u}\cdot\nabla T,w)+d(T,w)&=\langle q_{\mathrm{B}},w\rangle,\end{aligned}\tag{5}$$

where

$$a(\mathbf{u},\mathbf{v})=\int_\Omega \tau(\mathbf{u}):\nabla\mathbf{v}\,\mathrm{d}\Omega,\tag{6}$$

$$d(T,w)=\int_\Omega q(T)\cdot\nabla w\,\mathrm{d}\Omega\tag{7}$$

and the boundary terms are given by

$$\langle t^*,v\rangle=\int_{\partial K\setminus\Gamma_u}(\tau\cdot\hat{n}-p\hat{n})\cdot v\,\mathrm{d}s+\int_{\partial K\cap\Gamma_u}t^*\cdot v\,\mathrm{d}s,\tag{8}$$

$$\langle q_{\mathrm{B}},w\rangle=\int_{\partial K\setminus\Gamma_q}q\cdot nw\,\mathrm{d}s+\int_{\partial K\cap\Gamma_q}q_{\mathrm{B}}w\,\mathrm{d}s.\tag{9}$$

These variational equations are solved by a standard Galerkin finite element method coupled to an augmented Lagrangian algorithm to treat the incompressibility.[10] The equations are discretized using the seven-node triangular element which uses an enriched quadratic velocity field, a quadratic temperature and a linear discontinuous pressure approximation.[4,7]

3. ADAPTIVE METHODOLOGY

3.1. Generalities

The basic idea behind adaptive methods is to assess the quality of an initial solution obtained on a coarse mesh by using some form of error estimation and to modify the structure of the numerical approximation in a systematic fashion so as to improve the overall quality of the solution. There are several ways of achieving adaptivity: P-methods increase the degree of the polynomial approximation,[11] R-methods relocate grid points[12] and H-methods proceed by either mesh enrichment or remeshing.[1,3,4] Combinations such as H–P methods are also becoming popular.

A variant of an H-method, called adaptive remeshing, has been retained because it provides control of element size and grading to accurately resolve flow features such as shear and thermal layers. In this method the problem is first solved on a coarse grid to roughly capture the physics of the flow. The resulting solution is then analysed to determine where more grid points are needed and an improved mesh is generated. The problem is solved again on the new mesh using the solution obtained on the coarser mesh as an initial guess. This process is repeated until the required level of accuracy is achieved.

Remeshing also offers an elegant and simple approach to use the best-proven finite element approximations in an adaptive context.[10,13] This circumvents the problem associated with some P-methods of satisfying the so-called LBB compatibility condition between the velocity and pressure approximations while maintaining an optimal convergence rate. It also eliminates the 'hanging node problem' encountered in some H-refinement methods.[3]

3.2. Error estimation

This subsection describes two error estimation techniques for assessing the accuracy of the solutions obtained by the finite element solver.

3.2.1. A projection error estimator. This technique was first introduced in Reference 14 and is based on the observation that the diffusion fluxes of the finite element solution are discontinuous across element faces while the exact fluxes are continuous. The difference between the two is a measure of the accuracy of the numerical solution. The exact solution is obviously not known in cases of practical interest. However, an approximation to the true fluxes can be obtained by a least squares projection of the finite element fluxes. One can thus recover accurate estimates of the components of the shear stress tensor and heat flux vector. Let τ_{ij} and $\tilde{\tau}_{ij}$ be the finite (raw) and projected stresses. The least squares projection method seeks a continuous stress that minimizes the integral

$$\int_\Omega (\tau_{ij} - \tilde{\tau}_{ij})^2 \, \mathrm{d}\Omega. \tag{10}$$

The stresses are projected in the space of the velocity interpolation functions so that on each element one can write

$$\tilde{\tau}_{ij} = \sum_{i-1}^{6} \phi_n \{\bar{\tau}_{ij}\}_n. \tag{11}$$

Minimization of (10) leads to the variational equation

$$\sum_{K \in T} \left\{ \int_K \phi_m (\tau_{ij} - \tilde{\tau}_{ij}) \, \mathrm{d}\Omega \right\} = 0. \tag{12}$$

The nodal values of the continuous stresses are then obtained by solving the system

$$\left[\sum_{K \in T} \int_K \phi_m \phi_n \, \mathrm{d}\Omega \right] \{\bar{\tau}_{ij}\}_n = \left\{ \sum_{K \in T} \int_K \phi_m \tau_{ij} \, \mathrm{d}\Omega \right\}. \tag{13}$$

The same least squares projection approach is used to obtain a continuous approximation for the pressure and heat fluxes. The raw discontinuous linear pressure is projected in the space of linear continuous polynomials, while the heat flux is projected in the space of temperature interpolation functions. The velocity, pressure and temperature contributions to the error are then given by

$$e^u = \tilde{\tau} - \tau, \qquad e^p = \tilde{p} - p, \qquad e^T = \tilde{q} - q, \tag{14}$$

where the overtilde denotes a least squares projection.

The combined norms of the velocity, pressure and temperature fields and of their errors are computed using the expressions

$$\|(u, p, T)\| = (\|u\|_{\mathrm{E}}^2 + \|p\|_0^2 + \|T\|^2)^{1/2}, \tag{15}$$

$$\|(e^u, e^p, e^T)\| = (\|e^u\|_{\mathrm{E}}^2 + \|e^p\|_0^2 + \|e^T|^2)^{1/2}, \tag{16}$$

where the individual norms are defined as

$$\begin{aligned} \|u\|_{\mathrm{E}}^2 &= \int_\Omega \tau : \tau \ \mathrm{d}\Omega, & \|e^u\|_{\mathrm{E}}^2 &= \int_\Omega e^u : e^u \ \mathrm{d}\Omega, \\ \|p\|_0^2 &= \int_\Omega |p|^2 \ \mathrm{d}\Omega, & \|e^p\|_0^2 &= \int_\Omega |e^p|^2 \ \mathrm{d}\Omega, \\ \|T\| &= \int_\Omega q \cdot q \ \mathrm{d}\Omega, & \|e^T\|^2 &= \int_\Omega e^T \cdot e^T \ \mathrm{d}\Omega. \end{aligned} \tag{17}$$

Equation (15) is the so-called natural norm induced by the variational formulation of the problem, which includes variations in the fluid properties. This ensures that mesh refinement will occur in regions where heat flux and shear stress variations are significant. It will avoid overrefinement in cases where temperature and velocity may have steep gradients but fluid properties are small enough such that the heat fluxes and stresses show little variation. Notice that the norms used for velocity and temperature and for their errors involve only their derivatives. This ensures that the norm of the errors measures the accuracy of the velocity and temperature gradients. This is a natural approach to measure the accuracy of the skin friction coefficient and of the Nusselt number predictions.

It should be noted that in the present approach fluxes are projected rather than derivatives as is suggested in Reference 14. This ensures that the error estimator is well behaved in cases where physical properties are different in adjacent regions of the domain.[9] For this case the exact solution has discontinuous derivatives but a continuous conduction heat flux. Hence only the projection of fluxes makes sense in such situations.

3.2.2. A local PDE problem for the error. This approach provides an estimate of the error without having to solve the global least squares problems required by the previous estimator. Partial differential equations and their weak forms for the velocity, pressure and temperature errors can be derived directly from the Navier–Stokes equations.[5,15–17] Substitution of $u_{\mathrm{ex}} = u_h + e^u, p_{\mathrm{ex}} = p_h + e^p$ and $T_{\mathrm{ex}} = T_h + e^T$ into (5) yields the following variational problems for the errors:

$$\begin{aligned} a(e^u, v) - (e^p, \nabla \cdot v) &= -a(u, v) + (-\rho u_h \cdot \nabla u_h, v) + (p_h, \nabla \cdot v) + \langle [\tau \cdot n - p_h n]_{\mathrm{A}}, v \rangle_{\partial K \setminus \Gamma_i} + \langle \hat{t}, v \rangle_{\partial \cap \Gamma_i}, \\ (s, \nabla \cdot e^u) &= (s, \nabla \cdot u_h), \\ d(e^T, w) &= (-\rho c_{\mathrm{p}} u_h \cdot \nabla T_h, w) - d(T_h, w) + \langle q_{\mathrm{B}}, w >_{\partial K \cap \Gamma_T} + < [q_h \cdot n]_{\mathrm{A}}, w \rangle_{\partial K \setminus \Gamma_q}. \end{aligned} \tag{18}$$

The terms in parentheses on the right-hand side represent the element residuals, a measure of the accuracy of the finite element solution inside an element. The terms in brackets are the average momentum and heat fluxes across element faces. The difference between this average value and the finite element flux evaluated on the face of the element reflects how well the solutions on two neighbouring elements are matched. The second equation is a measure of mass conservation.

This variational problem is discretized locally on each element. Velocity and temperature errors are approximated with three quartic bubble functions (associated with the midside nodes of the triangle) obtained by squaring the midside node quadratic interpolation functions. The pressure error is approximated with an appropriate bubble function. This results in small 10×10 systems of equations which are inexpensive to solve. The norm of the errors is computed as in the previous section.

3.3. Adaptive remeshing

There remains to discuss how one exploits the knowledge of the error estimate distribution to design a better mesh. The adaptive remeshing strategy is straightforward. It follows that proposed in References 1, 4 and 5 and proceeds as follows.

1. Generate an initial mesh.
2. Compute finite element solution.
3. Compute error estimate.
4. If (global error < tolerance) then
   stop
   else
   compute grid density from error estimate
   generate an improved mesh using new grid density
   interpolate current solution on new mesh
   go to 2
   end if.

We now provide some details on this algorithm. Further details can be found in the work of Zienkiewicz and Zhu.[18] The procedure is as follows.

1. A target relative error is selected as $\eta_t\%$. The requirement is that $\eta < \eta_t$ at the end of the adaptive analysis.
2. The principle of equidistribution of the error is used to rewrite the above requirement as

$$\|e\|_i \leqslant e_{\text{av}} = \eta_t \left(\frac{\|u\|^2 + \|e\|^2}{m} \right)^{1/2}, \tag{19}$$

   where m is the number of elements in the mesh, e_{av} is the target element error and $\|e\|_i$ is the actual error on element i.
3. Elements with $\xi_i = \|e\|_i / e_{\text{av}} > 1$ are refined, while those with $\xi < 1$ are coarsened.
4. The element size required for the new mesh is obtained using the *a priori* asymptotic rate of convergence of the method:

$$\delta = h_i / \xi_i^{1/p}, \tag{20}$$

   where δ is the required element size on the new mesh, h_i is the current element size and p is the asymptotic rate of convergence of the finite element method. This expression for the element size can be rewritten as

$$\delta = \left[\eta_t \left(\frac{\|u\|^2 + \|e\|^2}{m} \right)^{1/2} \Big/ \|e\|_i \right]^{1/p} h_i. \tag{21}$$

   On most meshes the norm of the error is smaller than the norm of the solution, i.e.

$$\|e\| \ll \|u\|, \tag{22}$$

   which leads to the following expression for the new mesh size:

$$\delta = \left(\frac{\eta_t \|u\|}{\sqrt{m} \|e\|_i} \right)^{1/p} h_i. \tag{23}$$

We have described a very similar approach in Reference 4.

For linear differential operators this approach can in principle yield the required accuracy in one cycle of adaptation. However, results presented in Reference 18 indicate that this is not always the case. Dannelongue and Tanguy have observed a similar phenomenon for non-Newtonian flows.[19] Their numerical results show that it is more economical and cost-effective to use more than one step of adaptivity. A one-step remeshing strategy using the above algorithm leads to overly refined meshes in many regions, because the error estimate is necessarily an approximation to the true error. The error estimate and the rate of convergence of the finite element method hold asymptotically, i.e. on very fine meshes. Hence one can expect that the quality of the error estimate will be lower than expected on coarser meshes. Babuska[20] presents a theoretical analysis supporting this observation. He shows that introducing an intermediate step leads to a final mesh with fewer nodes to achieve the present level of accuracy η_t.

Dannelongue and Tanguy[19] apply this procedure recursively and use a sequence of meshes designed to achieve 12%, 1% and finally 0·1% relative error. Their transition operator, used to design the new mesh, is written as

$$\delta_i = \left(\frac{\bar{e}}{\|e_i\|}\right)^{1/p} h_i \tag{24}$$

and can by termed a 'fixed target' transition operator since the target η_t is fixed at the beginning of the adaptive process. The strategy proposed by Dannelongue and Tanguy amounts to changing η_t from one remeshing to the next. This is equivalent to reducing e_{av} by a predetermined factor. In Reference 18 this factor is approximately 10.

In the present work we adopt a similar approach. The element target error is defined as

$$\bar{e} = r\|e\|/\sqrt{n}, \tag{25}$$

where r is the error reduction factor, $\|e\|$ is the global error estimate and n is the number of elements in the mesh. After some manipulation we obtain the following expression for the new mesh size:

$$\delta_i = \left(\frac{r\|e\|}{\sqrt{n}\|e_i\|}\right)^{1/p} h_i. \tag{26}$$

We call this a 'reduction' transition operator since it attempts to reduce the total error by a factor r at each cycle of adaptation.

Both transition operators can be obtained from the expression

$$\delta_i = \left(\frac{\bar{e}}{\|e_i\|}\right)^{1/p} h_i \tag{27}$$

by defining $\bar{e}$ appropriately as follows:

(a) fixed target operator, $\bar{e} = \bar{\eta}\|u\|/\sqrt{n}$.
(b) reduction operator, $\bar{e} = r\|e\|/\sqrt{n}$.

As can be seen, for any target η_t in the fixed target operator there corresponds a value of r which will yield the same results using the reduction operator. In the present work we use values of r ranging from 0·5 to 0·3 which produce more gradual mesh refinement than the proposal of Reference 18. Our approach has proven to be especially cost-effective for solving steady state convection-dominated Navier–Stokes flows, because most of the iterations for non-linearities are carried out on the coarser meshes. The proposed more gradual approach produces two benefits. First, the final mesh has fewer nodes for the same accuracy achieved with a single step of adaptive remeshing. Second, the total cost for obtaining the solution on the final mesh is much lower that in the single-step approach. See Reference 4 for sample timings supporting this observation.

4. VALIDATION

The two error estimators are first compared on a simple flow problem for which an analytical solution is known. This provides controlled conditions to validate the proposed adaptive strategy and assess its computational performance.

The analytical solution of the problem was taken to be

$$\begin{aligned} &u = 1 - y^2, \qquad v = 0, \qquad p = x, \\ &T = [\cosh a - \cosh(ay)]/(\cosh a - 1). \end{aligned} \tag{28}$$

The constant a controls the thickness of the thermal boundary layer. In this problem only the temperature field will contribute to the error, since the finite element approximation provides an exact representation of the velocity and pressure fields. The problem is solved on the unit square. The adaptive strategy is set to reduce the computed error by a factor of three at each cycle. Tables I and II illustrate the performance of the adaptive strategy for both the projection and local problem error estimators. As can be seen, both the true error and its estimate are reduced at each cycle. Hence, the solution accuracy improves steadily at each adaptation cycle. In general, starting from a coarse mesh and requesting a reduction of the error estimate by a factor of three at each cycle, one usually obtains an order-of-magnitude reduction of the true error after three cycles. One seldom obtains a reduction by a factor of 27 (3^3) on the third mesh, because the asymptotic rate of convergence of the finite element method does not formally hold on the initial coarse grid. This rate is achieved only for finer meshes (hence the qualifier asymptotic). In practice the factor of three is nearly recovered when the initial mesh is fine enough or if further cycles of adaptations are performed.

As can be seen, both methods lead to comparable meshes and true errors of similar magnitude. Note, however, that the local problem approach produces more accurate error estimates. This approach was originally introduced as a cost-effective alternative to the projection method since it does not involve the solution of the global least squares problem. However, in practice the higher-order Gaussian quadrature rules required to evaluate the coefficients of the 10×10 system makes this approach somewhat more expensive than the projection method.

5. APPLICATION

5.1. Forced convection with transverse injection in a sudden expansion

This configuration, studied in Reference 21, is shown in Figure 1. Laminar flow enters the backward-facing step whose bottom walls (2 and 5) and step (3) are heated at a constant temperature. The top wall is adiabatic and fluid can be injected with a velocity v_j at the base of the step through an opening (4). Simulations were performed for the two cases studied in Reference 21 at a Reynolds number of 100: 1, forced convection, no injection, $v_j = 0$; 2, forced convection with injection, $v_j = 0{\cdot}2$.

Table I. 1D case, projection estimator

Mesh	No. of nodes	No. of elements	Error estimate	True error
0	347	106	0·03327	0·1070
1	587	187	0·009959	0·03079
2	1135	361	0·006189	0·01412
3	1589	514	0·003254	0·007732

Table II. 1D case, local problem estimator

Mesh	No. of nodes	No. of elements	Error estimate	True error
0	347	106	0·09737	0·1070
1	421	134	0·02924	0·04832
2	945	306	0·01264	0·01831

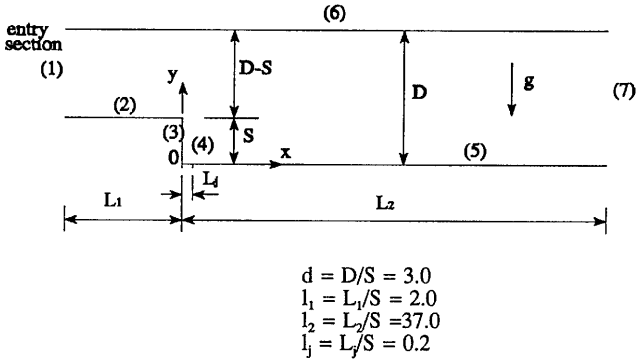

Figure 1. Forced convection with injection: computational domain

Case 1. No Injection. Figure 2 shows the sequence of meshes generated by the adaptive strategy set to reduce the error by a factor of three at each cycle of adaptation. As can be seen, the grid is progressively refined in the thermal layer on the bottom wall upstream of the step and in the shear layers present on the top wall and emanating from the corner. The isotherms and streamlines shown in Figure 3 are in excellent agreement with those of Soong and Hsueh.[21]

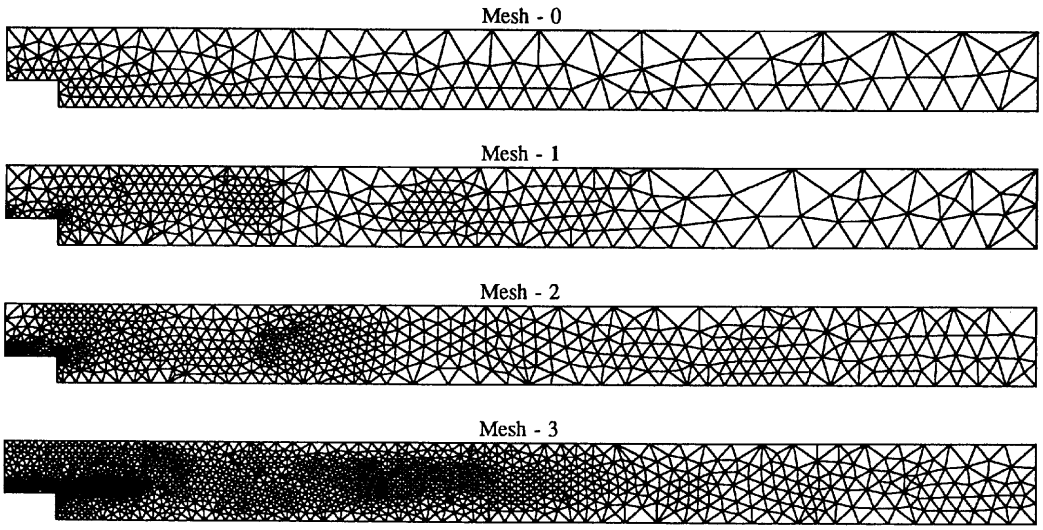

Figure 2. Meshes generated for Case 1: no injection

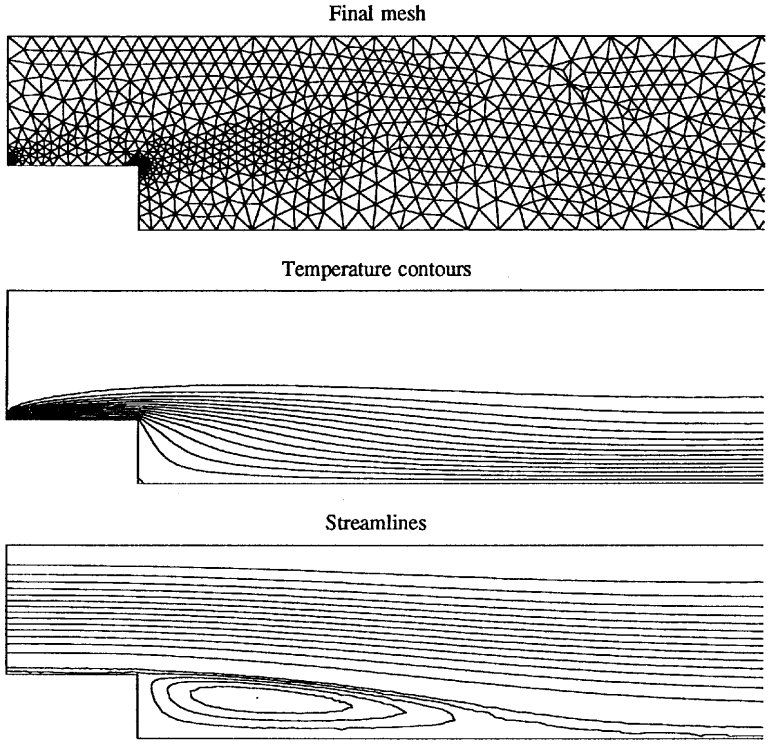

Figure 3. Final mesh, isotherms and streamlines for Case 1

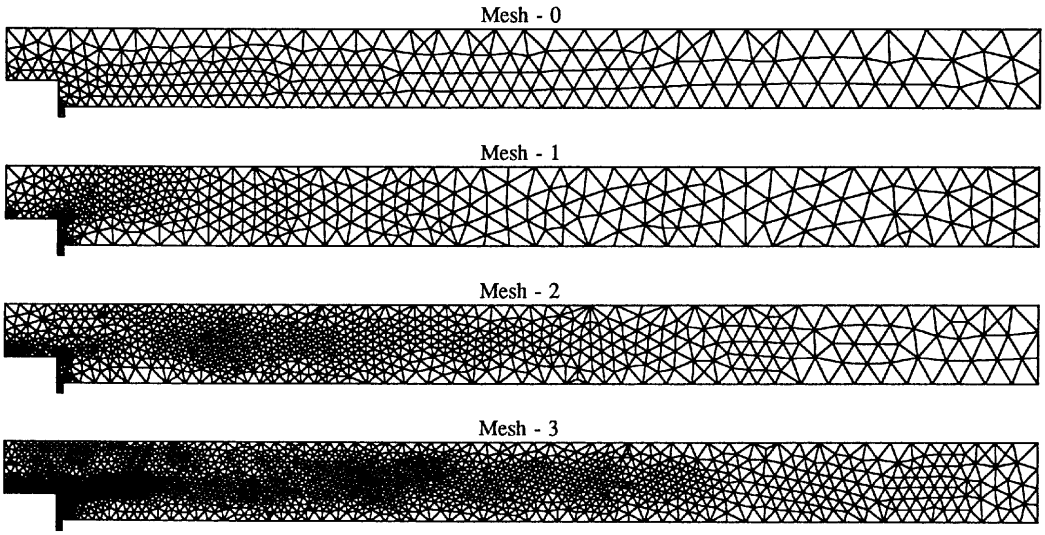

Figure 4. Meshes generated for Case 2: with injection

Case 2. Forced convection with cold fluid injection. Fluid is injected vertically at the base of the step with a velocity $v_j = 0{\cdot}2\bar{U}$, where $\bar{U}$ is the mean velocity at the channel inflow. Meshes are shown in Figure 4 and isotherms and streamlines in Figure 5. As can be seen, refinement occurs near the corner, near the injection point and on the base of the step where fluid injection causes a thin wall shear layer.

The isotherms show the significant cooling effect due to injection. The streamline plot also shows the changes in the shape, extent and topology of the recirculation zone. Figures 6 and 7 compare the Nusselt number predictions obtained on the adaptively generated meshes with and without injection respectively. As can be seen, grid-independent results have been obtained at the third cycle of adaptation.

5.2. *Forced convection in a grooved duct*

This configuration was studied experimentally and numerically in Reference 22. Figure 8 presents a sketch of the domain with boundary conditions. The channel walls are maintained at constant but different temperatures. The grooved wall on top is heated, while the bottom wall is maintained at the inlet temperature.

The problem results in a thermal boundary layer that is periodically interrupted by grooves. The flow separates leaving recirculation zones inside the grooves so that the thermal boundary layer must redevelop after each groove. The effect is to increase the heat transfer coefficient when compared with the parallel plate duct case. The grooves have an aspect ratio $w/h = 4$, where h is half the height of the duct. The Reynolds number is based on the mean velocity u_m and the hydraulic diameter

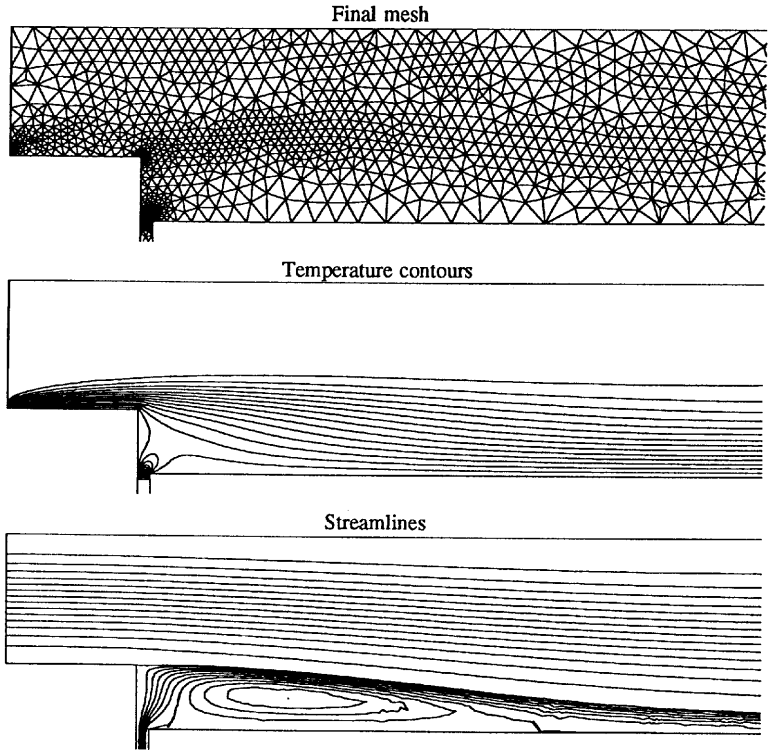

Figure 5. Final mesh, isotherms and streamlines for Case 2

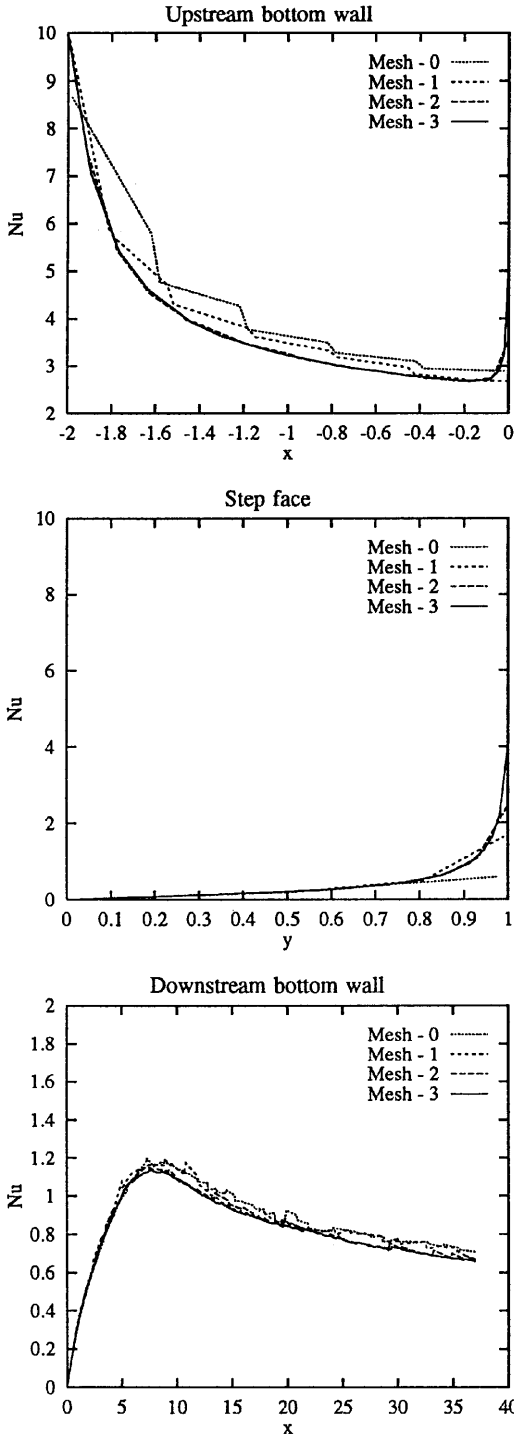

Figure 6. Nusselt number distribution for Case 1: no injection

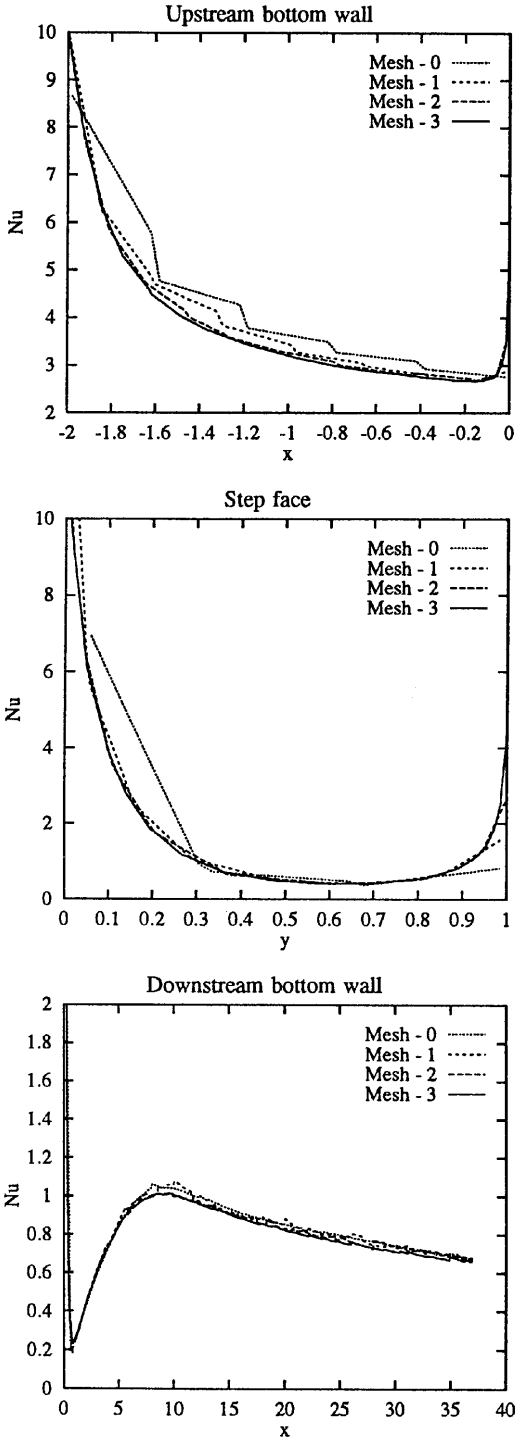

Figure 7. Nusselt number distribution for Case 2: with injection

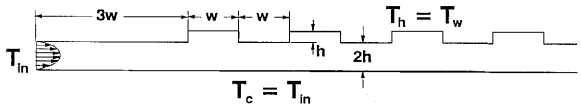

Figure 8. Grooved duct: computational domain and boundary conditions

$D_h = 6h$. Simulations were performed for air ($Pr = 0{\cdot}72$) at different Reynolds numbers ranging from 620 to 1760.

Solutions have been obtained on adaptive meshes by using both the postprocessing and local problem error estimators. Tables III–X summarize the performance of the adaptivity strategy for Reynolds numbers of 620, 1076, 1481 and 1760. Both estimators produce a reduction of the error at each cycle by a factor which is not too far from the requested value of three. Hence the solution accuracy improves steadily at each adaptation cycle.

Figures 9–12 show for each Reynolds number the initial and final meshes, along with streamlines and contour plots of the temperature. As can be seen, the shear and boundary thermal layers become thinner with increasing Reynolds number.

Table III. Grooved duct, $Re = 620$, projection estimator

Mesh	No. of nodes	No. of elements	Solution norm	Error estimate
0	1040	449	1·165	$1{\cdot}400 \times 10^{-2}$
1	1668	777	1·169	$5{\cdot}859 \times 10^{-3}$
2	2508	1179	1·158	$3{\cdot}138 \times 10^{-3}$
3	4111	1962	1·153	$1{\cdot}615 \times 10^{-3}$
4	7313	3538	1·152	$8{\cdot}758 \times 10^{-4}$

Table IV. Grooved duct, $Re = 620$, local problem

Mesh	No. of nodes	No. of elements	Solution norm	Error estimate
0	1040	449	1·165	$1{\cdot}290 \times 10^{-2}$
1	1514	699	1·158	$5{\cdot}258 \times 10^{-3}$
2	2575	1204	1·161	$2{\cdot}689 \times 10^{-3}$
3	4436	2101	1·152	$1{\cdot}299 \times 10^{-3}$
4	8303	3982	1·152	$6{\cdot}239 \times 10^{-4}$

Table V. Grooved duct, $Re = 1076$, projection estimator

Mesh	No. of nodes	No. of elements	Solution norm	Error estimate
0	1040	449	0·6775	$9{\cdot}733 \times 10^{-3}$
1	1527	704	0·6808	$4{\cdot}116 \times 10^{-3}$
2	2677	1248	0·6738	$1{\cdot}699 \times 10^{-3}$
3	4837	2292	0·6670	$8{\cdot}528 \times 10^{-4}$
4	8784	4207	0·6667	$4{\cdot}251 \times 10^{-4}$

Table VI. Grooved duct, $Re = 1076$, local problem

Mesh	No. of nodes	No. of elements	Solution norm	Error estimate
0	1040	449	0·6775	$1{\cdot}615 \times 10^{-2}$
1	1734	805	0·6746	$7{\cdot}667 \times 10^{-3}$
2	2558	1209	0·6761	$4{\cdot}334 \times 10^{-3}$
3	3714	1773	0·6690	$1{\cdot}782 \times 10^{-3}$
4	6308	3045	0·6668	$8{\cdot}611 \times 10^{-4}$

Table VII. Grooved duct, $Re = 1481$, projection estimator

Mesh	No. of nodes	No. of elements	Solution norm	Error estimate
0	1040	449	0·4913	$8{\cdot}762 \times 10^{-3}$
1	1591	734	0·4872	$6{\cdot}483 \times 10^{-3}$
2	1967	908	0·4863	$2{\cdot}357 \times 10^{-3}$
3	3681	1732	0·4883	$1{\cdot}099 \times 10^{-3}$
4	6352	3029	0·4840	$5{\cdot}294 \times 10^{-4}$

Table VIII. Grooved duct, $Re = 1481$, local problem

Mesh	No. of nodes	No. of elements	Solution norm	Error estimate
0	1040	449	0·4913	$1{\cdot}802 \times 10^{-2}$
1	1861	868	0·4989	$8{\cdot}926 \times 10^{-3}$
2	2516	1191	0·4915	$4{\cdot}208 \times 10^{-3}$
3	3708	1775	0·4840	$1{\cdot}931 \times 10^{-3}$
4	6211	3004	0·4846	$9{\cdot}628 \times 10^{-4}$

Table IX. Grooved duct, $Re = 1760$, projection estimator

Mesh	No. of nodes	No. of elements	Solution norm	Error estimate
0	1040	449	0·4133	$8{\cdot}395 \times 10^{-3}$
1	1628	751	0·4144	$5{\cdot}741 \times 10^{-3}$
2	2168	1003	0·4082	$2{\cdot}383 \times 10^{-3}$
3	4012	1899	0·4090	$1{\cdot}207 \times 10^{-3}$
4	6064	2891	0·4067	$5{\cdot}450 \times 10^{-4}$

Table X. Grooved duct, $Re = 1760$, local problem

Mesh	No. of nodes	No. of elements	Solution norm	Error estimate
0	1040	449	0·4133	$1{\cdot}915 \times 10^{-2}$
1	1875	874	0·4146	$9{\cdot}118 \times 10^{-3}$
2	2889	1372	0·4143	$4{\cdot}421 \times 10^{-3}$
3	4368	2101	0·4097	$1{\cdot}803 \times 10^{-3}$
4	7044	3421	0·4074	$1{\cdot}008 \times 10^{-3}$

Figures 13–15 show predictions of the Nusselt number along the grooved wall, along with the computations and measurements of Farhanieh *et al.*[22] As can be seen, grid-independent results have been obtained for all cases studied. Furthermore, predictions compare extremely well with measurements. This is especially evident near the protruding and re-entrant corners. The sharp increase in Nusselt number near the upstream-facing corners is very well captured. This is especially true at higher Reynolds numbers. The case of the re-entrant corner is also very indicative of the performance of the adaptive strategy. Because the temperature is constant on the heated wall, the Nusselt number must be zero at the top corners of the groove. The predicted values capture this measured phenomenon very well: sharp peaks and dips are very well reproduced by the present

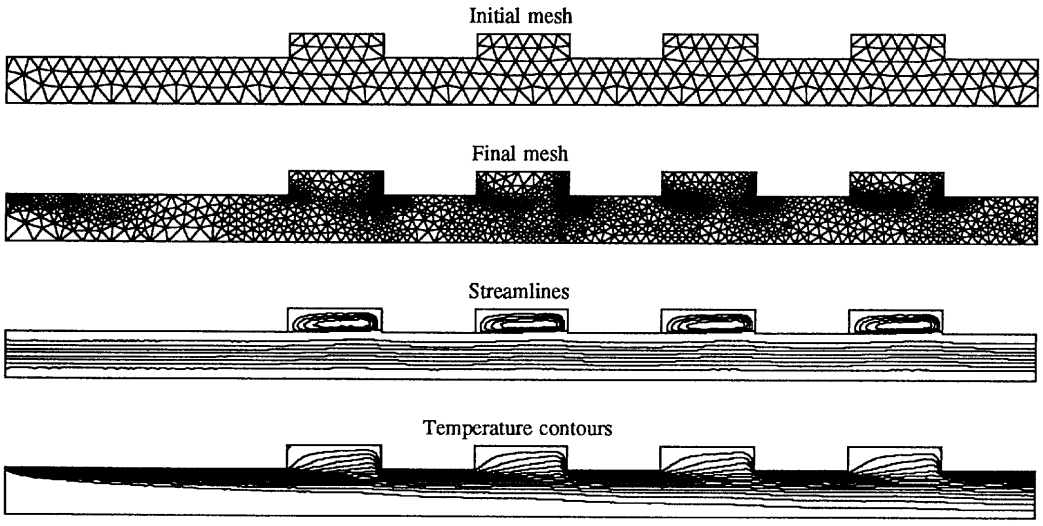

Figure 9. First and final meshes, streamlines and temperature contours, $Re = 620$

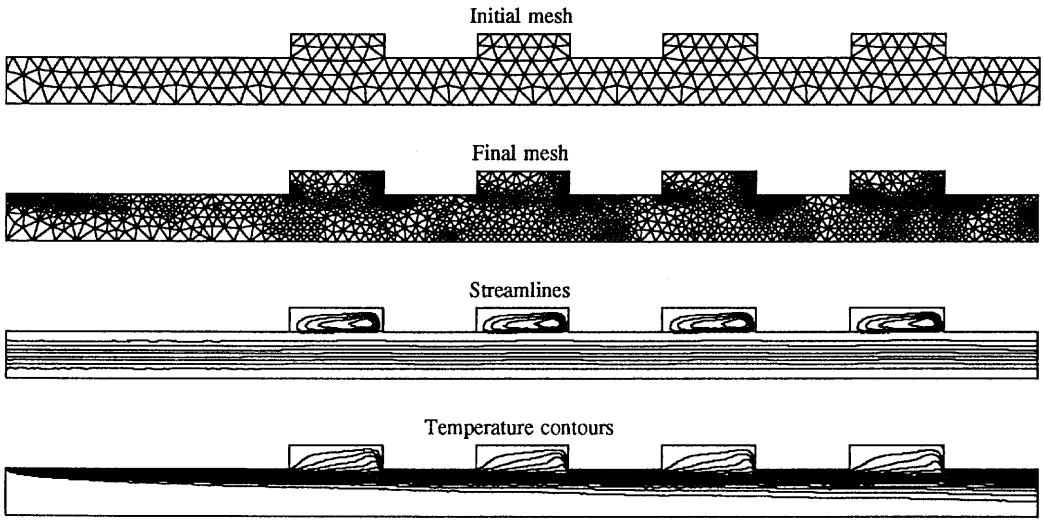

Figure 10. First and final meshes, streamlines and temperature contours, $Re = 1076$

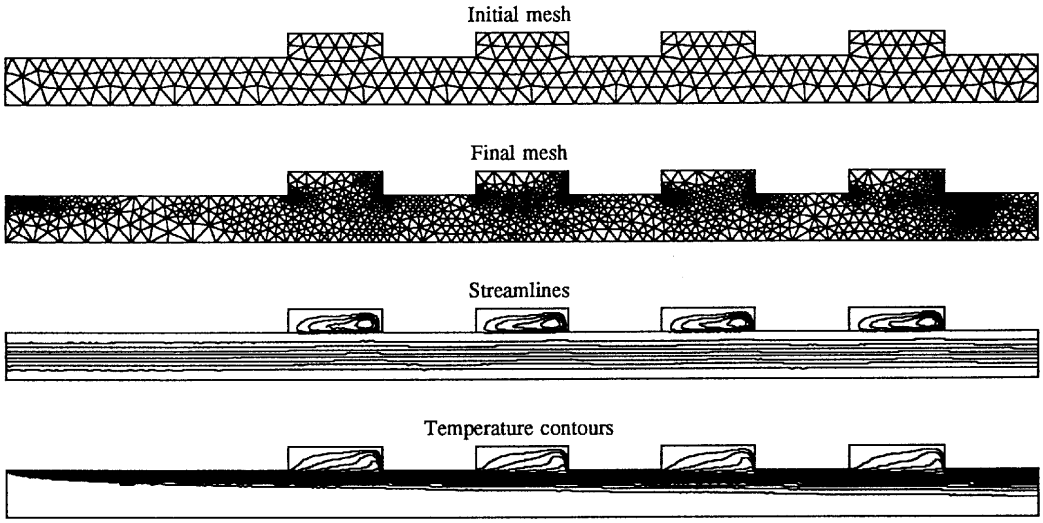

Figure 11. First and final meshes, streamlines and temperature contours, $Re = 1481$

method, while the finite volume method of Farhanieh *et al.*[22] totally misses the peaks and dips for all Reynolds numbers except the lowest one.

5.3. *Computational efficiency*

Results presented in the preceding subsection illustrate the improved resolution that can be achieved with adaptivity. The proposed adaptive strategy also results in a cost-effective solution algorithm that is well worth the added complexity. Table XI contains computational statistics obtained on an IBM E/S 9000 with vector facility, for forced convection without injection, using the

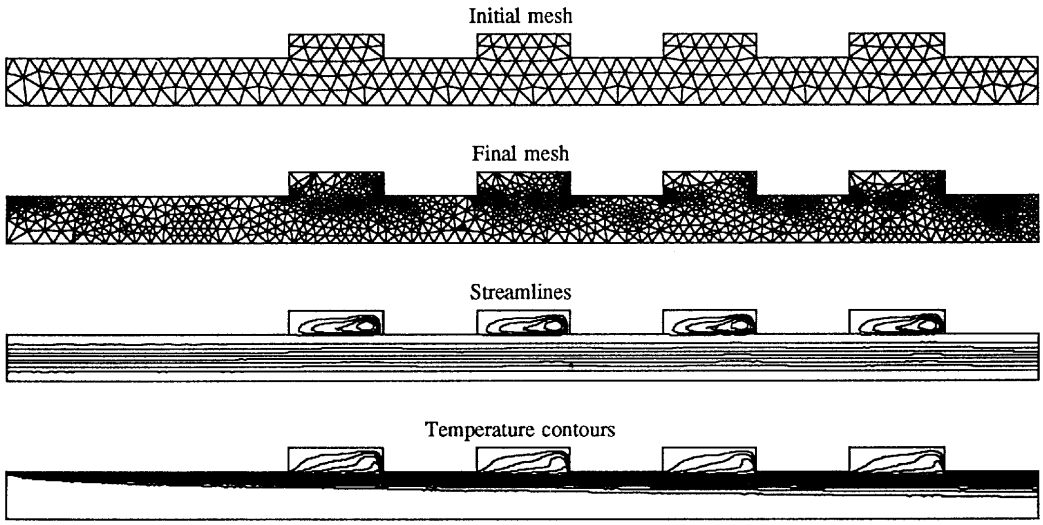

Figure 12. First and final meshes,a streamlines and temperature contours $Re = 1760$

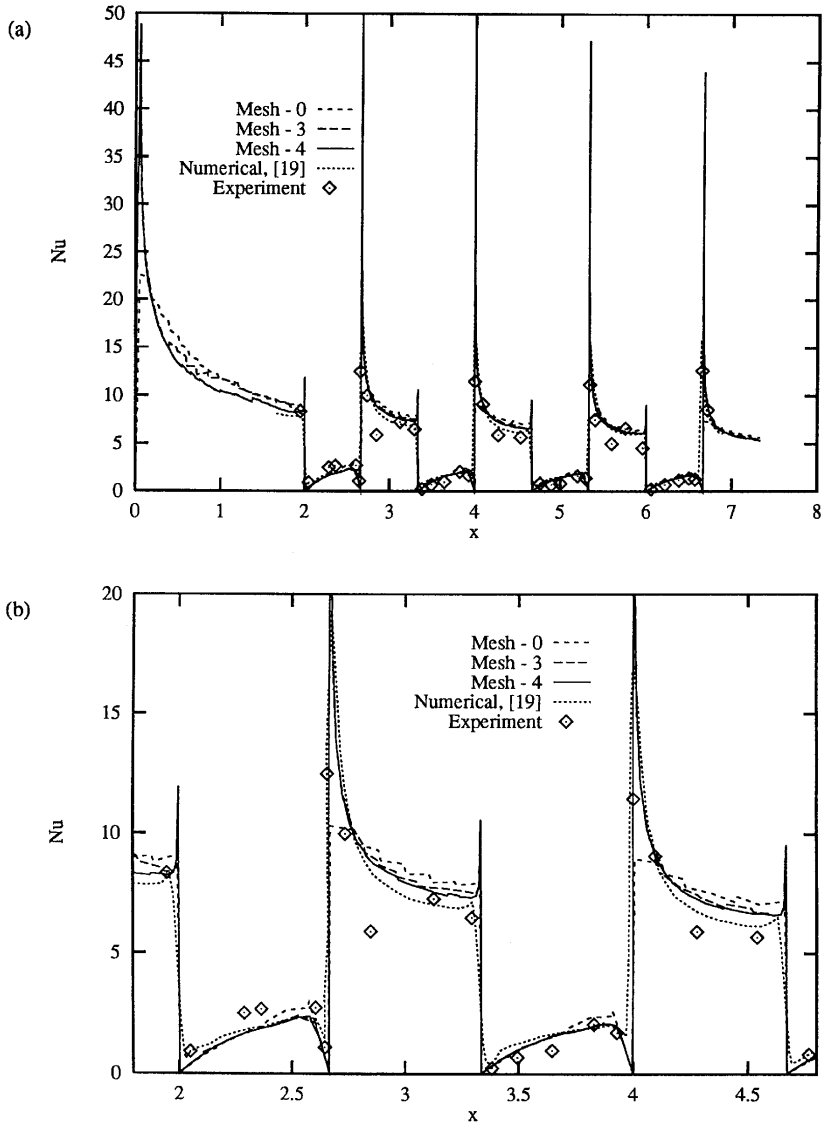

Figure 13. Local Nusselt number distribition on heated wall, $Re = 620$: (a) global view; (b) detail of distribution

Table XI. Computational statistics for adaptation

Cycle	No. of iterations	Meshing (s)	Solution (s)	Adaptation (s)
0	10	0·27	4·50	0·70
1	6	1·21	9·82	1·50
2	4	2·00	19·91	3·11
3	4	3·79	63·39	6·43
4	3	8·05	80·50	12·15
5	3	18·93	465·61	32·61

projection estimator. Timings, in seconds, include all aspects of computations (grid generation, flow solution, error estimation and interpolation of the solution between grids).

Computation of the error estimate represents typically less than 5% of the cost of obtaining a solution on a given mesh. Complete solution of this problem required a total of 735 CPU seconds. Solving the same problem directly on the final mesh without using intermediate grids would have required approximately 1550 CPU seconds.

It should also be noted that without adaptivity it would have been nearly impossible to generate a grid leading to comparable accuracy without at least doubling the number of grid points on the final

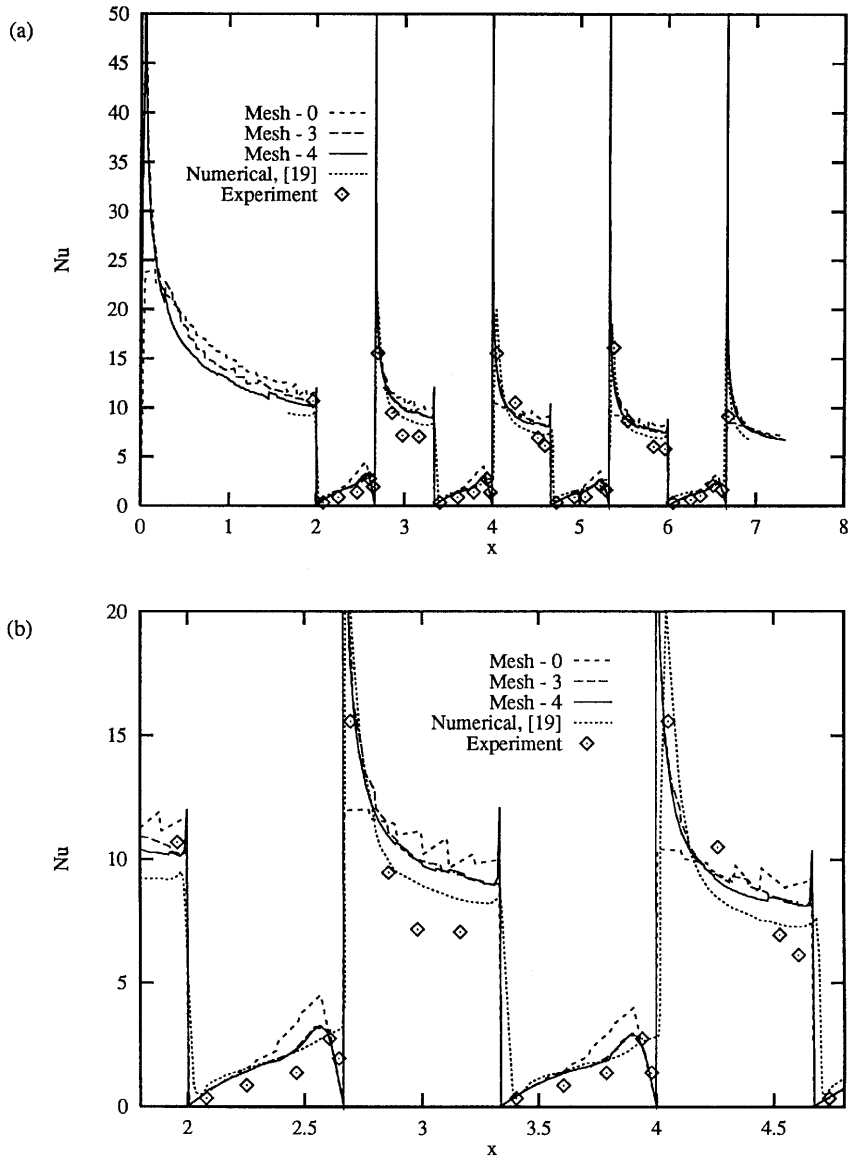

Figure 14. Local Nusselt number distribution on heated wall, $Re = 1076$: (a) global view; (b) detail of distribution

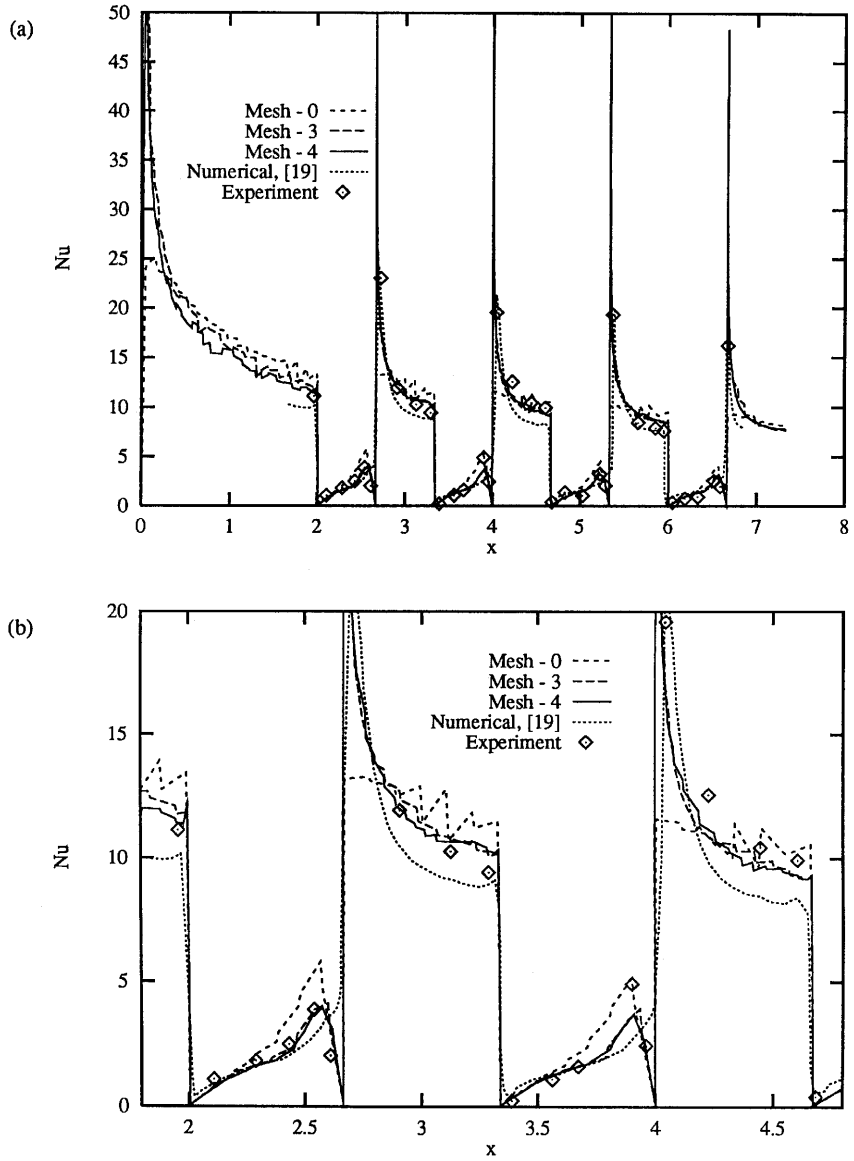

Figure 15. Local Nusselt number distribution on heated wall, $Re = 1481$: (a) global view; (b) detail of distribution

mesh. In fact, it is very difficult to achieve a good allocation of grid points without the extra knowledge gained from the error estimates. Given that Gaussian elimination is used at each Newton iteration, the increase in computational cost is proportional to the cube of the number of grid points. It follows that non-adaptive computations of comparable accuracy would have been far more expensive than adaptive ones (our experience indicates that a factor of five is realistic and is a conservative estimate).

6. CONCLUSIONS

An adaptive remeshing finite element procedure has been presented for solving forced convective heat transfer problems. The two error estimators presented have proven reliable and convergent on problems with known analytical solutions. Both estimators are sensitive to hydrodynamic and thermal layers. The adaptive procedure has proven robust and can be used effectively in a black-box fashion with little or no intervention on the part of the user. Predictions of Nusselt number distributions are in excellent agreement with experiment and constitute an improvement over other traditional computations.

ACKNOWLEDGEMENTS

This work was supported in part by the National Science and Engineering Research Council of Canada and by Le Fonds FCAR de la Province de Québec. The authors would like to express gratitude to Frédéric Tran-Khanh for his assistance in producing some of the numerical results.

REFERENCES

1. J. Peraire, M. Vahdati, K. Morgan and O. C. Zienkiewicz, 'Adaptive remeshing for compressible flows', *J. Comput. Phys.*, **72**, 26–37 (1987).
2. J. Wu, J. Z. Zhu, J. Szmelter and O. C. Zienkiewicz, 'Error estimation and adapativity in Navier–Stokes incompressible flows', *Comput. Mech.*, **6**, 259–270 (1990).
3. K. C. Wang and G. F. Carey, 'Adaptive grids for coupled viscous flow and transport', *Comput. Methods Appl. Mech. Eng.*, **82**, 365–383 (1990).
4. J. F. Hétu and D. Pelletier, 'Adapative remeshing for viscous incompressible flows', *AIAA* J., **30**, 1986–1992 (1992).
5. J.-F. Hétu and D. Pelletier, 'A fast adaptive finite element scheme for viscous incompressible flows', *AIAA J.*, **30**, 2677–2682 (1992).
6. D. Pelletier and J.-F. Hétu, 'An adaptive finite element methodology for incompressible viscous flows', in *Advances in Finite Elements for Fluid Dynamics II*, FED Vol. 137, ASME, New York, 1992, pp. 1–12.
7. D. Pelletier, J.-F. Hétu and F. Ilinca, 'Adaptive finite element method for thermal flow problems', *AIAA J.*, **32**, 741–747 (1994).
8. D. Pelletier, F. Ilinca and J.-F. Hétu, 'An adaptive finite element method for turbulent free shear flow past a propeller', *AIAA J.*, **32**, 2186–2193 (1994).
9. D. Pelletier, F. Ilinca and J.-F. Hétu, 'Adaptive remeshing for convective heat transfer with variable fluid properties', *AIAA J. Thermophys. Heat Transfer*, **8**, 687–694 (1994).
10. D. Pelletier and A. Fortin, 'Are FEM solutions of incompressible flows really incompressible? (or how simple flows can cause headaches)', *Int. j. numer. methods fluids*, **9**, 99–112 (1989).
11. O. C. Zienkiewicz, J. P. Gago and D. W. Kelley, 'The hierarchical concepts in finite element analysis', *Comput. Struct.*, **16**, 53–65 (1983).
12. R. Lohner, K. Morgan and O. C. Zienkiewicz, 'Adaptive grid refinement for the Euler and compressible Navier–Stokes equations', in I. Babuska, O. C. Zienkiewicz and E. R. de A. Oliveira (eds), *Accuracy Estimates and Adaptive Refinement in Finite Element Computations*, pp. 281–248, Wiley, Chichester, 1986.
13. M. Fortin and A. Fortin, 'Experiments with several elements for incompressible flows', *Int. j. numer. methods fluids*, **5**, 911–928 (1985).
14. O. C. Zienkiewicz and R. J. Z. Zhu, 'A simple error estimator and adaptive procedure for practical engineering analysis', *Int. j. numer. methods eng.*, **24**, 337–357 (1987).
15. J. F. Hétu, 'Méthode d'éléments finis adaptatives pour les écoulements visqueux incompressibles', ;Thèse de Ph.D., École Polytechnique de Montréal, 1991.
16. J. T. Oden, L. Demkowicz, T. Strouboulis and P. Devloo, 'Adapative methods in solid and fluid mechanics', in I. Babuska, O. C. Zienkiewicz and E. R. de A. Oliveira (eds), *Accuracy Estimates and Adaptive Refinement in Finite Element Computations*, pp. 249–280, Wiley, Chichester, 1986.
17. J. T. Oden, 'The best FEM', *Finite Elem. Anal. Design*, **7**, 103–114 (1990).
18. O. C. Zienkiewicz and R. J. Z. Zhu, 'A simple error estimator and adaptive procedure for practical engineering analysis', *Int. j. numer. methods eng.*, **24**, 337–357 (1987).
19. H. H. Dannelongue and P. A. Tanguy, 'Adapative remeshing technique for Non-Newtonian fluid flow', *Int. j. numer. methods eng.*, **30**, 1555–1567 (1990).

20. I. Babuska, 'Feedback, adaptivity and *a posteriori* estimates in finite elements: aims, theory, and experience', in I. Babuska, O. C. Zienkiewicz and E. R. de A. Oliveira (eds), *Accuracy Estimates and Adaptive Refinement in Finite Element Computations*, Wiley, Chichester, 1986.
21. C. Y. Soong and W. C. Hsueh, 'Mixed convection in a suddenly-expanded channel with effects of cold fluid injection', *Int. J. Heat Mass Transfer*, **36**, 1477–1484 (1993).
22. B. Farhanieh, C. Herman and B. Sundu, 'Numerical and experimental analysis of laminar fluid flow and forced convection heat transfer in a grooved duct', *Int. j. Heat Mass Transfer*, **36**, 1609–1617 (1993).

